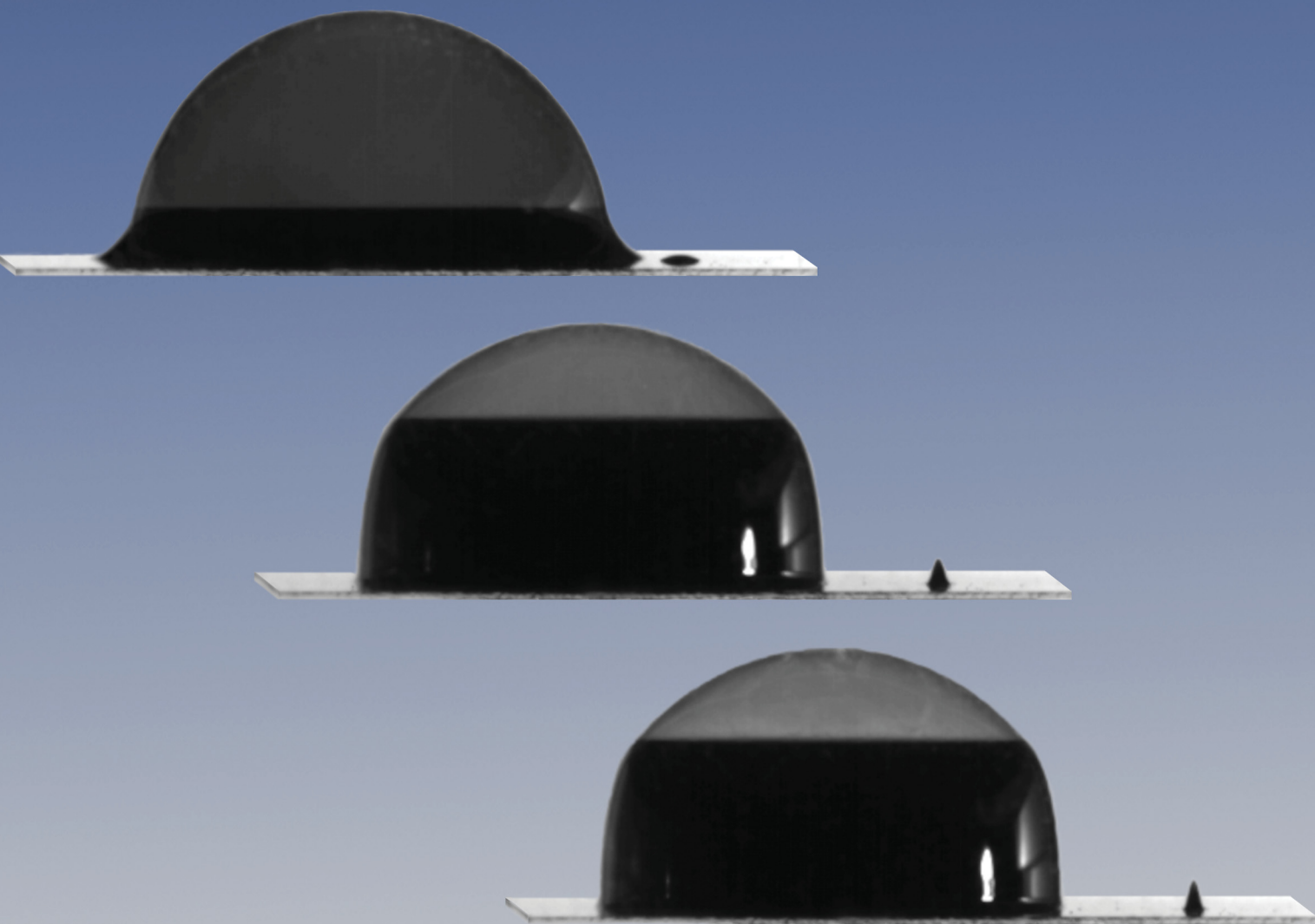


# Soft Matter

[rsc.li/soft-matter-journal](https://rsc.li/soft-matter-journal)



ISSN 1744-6848


 Cite this: *Soft Matter*, 2023, 19, 8318

 Received 17th July 2023,  
Accepted 9th October 2023

DOI: 10.1039/d3sm00936j

[rsc.li/soft-matter-journal](https://rsc.li/soft-matter-journal)

## Deformation of soap bubbles in uniform magnetic fields

 S. Mawet,<sup>a</sup> H. Caps,<sup>a</sup> S. Dorbolo,<sup>b</sup> and F. Elias<sup>c</sup>

The deformation of hemispherical sessile bubbles made of ferrofluid soap under vertical uniform magnetic fields was studied using Helmholtz coils. The deformation and the shape of the bubbles were monitored according to the amplitude of the magnetic field, the initial volume of the bubbles and the ferrofluid volume used to create them. The meniscus was found to bear most of the deformation, reshaping into a cylinder, with the remainder of the bubble forming a spherical cap, mainly adapting to the meniscus transformation. The growth of the meniscus height was rationalised using a simple model. More precisely, the meniscus shape depends on the competition between capillary, gravity and magnetic effects. These three ingredients can be rewritten to highlight two characteristic lengths of the system: the capillary and the magnetic lengths. Depending on the magnetic field intensity, the shape of the meniscus is described by one of the two lengths, thus revealing the existence of two distinct regimes.

### 1. Introduction

Sessile and floating bubbles are pockets of gas enclosed inside a thin liquid film. Due to surface tension, they naturally adopt a spherical shape which can be modified by the application of an external field. Indeed, in the gravity field, Cohen *et al.*<sup>1</sup> showed that metric-sized sessile bubbles are flattened, while Teixeira *et al.*<sup>2</sup> demonstrated that the shape of floating bubbles is determined by buoyancy. Moreover, the application of a uniform electric field on a floating or sessile bubble made of a conducting liquid induces its deformation into an ellipsoid (see Fig. 1(a)) or, for a field higher than a critical one, into a cone, the well-known Taylor cone.<sup>3–5</sup> In this paper, we show that a uniform magnetic field can also be used to reshape a bubble made of a solution containing a ferrofluid<sup>6,7</sup> and a surfactant, forming a ferrofluid soap.<sup>8,9</sup> An example of such a deformation is illustrated in the pictures in Fig. 1(b). Unlike gravity and the electric field, which reshape the whole bubble, the magnetic field acts mainly on the meniscus of the bubble, increasing the meniscus height as its intensity rises. The aim of this paper is to rationalise and explain these deformations.

Ferrofluids are stable colloidal dispersions of ferromagnetic nanoparticles in a carrier liquid. In general, the effect of an external magnetic field on such a ferrofluid body is twofold. If the field is not uniform, a volumetric magnetic force is applied

to the body and can, for instance, compensate the gravity force.<sup>10</sup> If the magnetic field is uniform, the alignment of the magnetic moments carried by the particles generates a dipolar repulsion between the particles, which results in a deformation of the body.<sup>7,11</sup> The effect of the two magnetic forces can be illustrated by several phenomena. For example, beyond a certain critical threshold, a flat and still ferrofluid surface subjected to a perpendicular uniform magnetic field  $\vec{B}_0$  deforms due to a peak instability: the so-called Rosensweig instability.<sup>12,13</sup> Inside a two-phase liquid, a uniform magnetic field can also deform the ferrofluid droplets forming one of the phases, stretching them in the direction of the field.<sup>14</sup> Moreover, when such a two-phase liquid is confined, many different patterns can emerge.<sup>15</sup>

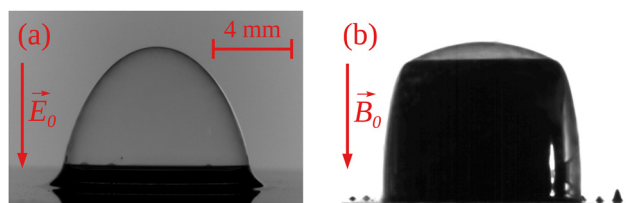


**Fig. 1** Pictures of bubbles resting on horizontal solid substrates subjected to a vertical uniform electric (a) and magnetic (b) field. The internal gas volumes are identical in both cases:  $V_g = 0.5$  mL. Image (a) shows a bubble on a conductive plate under an electric field intensity  $E_0 = 480$  V mm<sup>-1</sup> generated by a plane capacitor of 25 mm thick. The bubble consists of conductive soap and assumes a hemi-spheroidal shape due to the charges attraction.<sup>3</sup> Picture (b) depicts the shape of a bubble on a microscopic slide under a magnetic field with an intensity of  $B_0 = 41.22$  mT. The bubble is made up of a volume of soapy ferrofluid  $V_{ff} = 60$   $\mu$ L and adopts the shape of a cylinder closed by a thin spherical cap due to dipole alignment. The scale of both pictures is approximately the same and is indicated in the upper right-hand corner of image (a).

<sup>a</sup> CESAM Research Unit, University of Liège, B-4000 Liège, Belgium.  
E-mail: smawet@uliege.be

<sup>b</sup> GRASP Lab, CESAM Research Unit, University of Liège, B-4000 Liège, Belgium

<sup>c</sup> PMMH, CNRS, ESPCI Paris, Université PSL, Sorbonne Université, Université Paris Cité, F-75005 Paris, France

Deformations due to a magnetic field can also be observed on ferrofluid droplets resting on a superhydrophobic substrate, as investigated by Timonen *et al.*<sup>16</sup> thanks to a non-uniform magnetic field produced by a permanent magnet. They not only found that droplets deform into a conical spiked shape, but also that they may divide due to the non-uniformity of the magnetic field. Later, Rigoni *et al.*<sup>17</sup> showed that ferrofluid droplets can either be flattened by magnetic interaction due to the magnetic gradient or elongated by a uniform magnetic field. Both phenomena result from the competition between a magnetic pressure, which tends to deform the droplet, and the capillary one, trying to keep it spherical. Later, Rigoni *et al.*<sup>18</sup> showed that these competitions can also be used to describe the separation of a ferrofluid droplet into daughter ones. Latikka *et al.*<sup>19</sup> further studied the separation in daughter droplets and observed the presence of satellite and subsatellite droplets after splitting. Furthermore, they also investigated the impact of both the substrate and ferrofluid composition on the self-assembled pattern induced by the separations. Shyam *et al.* have also shown that a time-dependent magnetic field can be used to enhance the convective flow within a drop to both increase its evaporation rate<sup>20</sup> and the mixing between two fluids of different magnetic susceptibilities.<sup>21</sup>

In the work reported in this article, the ferrofluid is confined between the liquid–air interfaces of a soap bubble deposited on a solid surface. The bubble is hemispherical and a liquid meniscus borders the equatorial line at the junction between the bubble and the solid substrate. Whereas the thickness of the bubble soap film is usually of the order of a micrometre or less, most of the fluid volume lies in the meniscus, which is millimetre thick. The application of a vertical external uniform magnetic field induces growth in the height of the meniscus. This growth presents both similarities and differences with the Rosensweig instability and the ferrofluid droplet deformation. On one hand, the effect of a uniform magnetic field seems to induce a rise of the ferrofluid in each case. Yet, on the other hand, for the magnetic field intensities tested, the meniscus does not deform into spikes nor separate beyond a critical field. It forms a cylinder whose height grows with the intensity of the magnetic field (see Fig. 2). This ferrofluid cylinder holds until the bubble blows up, at which point the ferrofluid separates into small droplets as a drop subjected to a sufficiently high magnetic field does.<sup>18</sup> This reaction means that the bubble not only forces the liquid volume into a singular shape, *i.e.* a meniscus topped by a thin liquid cap, but also holds it together, preventing it from separating under the action of the magnetic field.

Other studies have already explored the interaction between a meniscus and an applied magnetic field, but none of them fully explain the behaviour of the bubble meniscus. For example, Rosensweig<sup>7</sup> (see the application on the conical meniscus at the end of the fifth chapter on pages 79 to 82 of ref. 7) also observed the growth of a meniscus, formed around a wire emerging vertically from a ferrofluid pool, with the applied magnetic field. He shows that the height is prescribed by the competition between the magnetic and the gravity fields. However, the conclusions drawn from this situation do not remain valid in the case of a ferrofluid bubble. Indeed, neither the meniscus nor

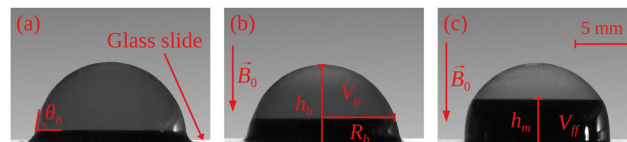


Fig. 2 Pictures of a bubble resting on a horizontal microscopic slide glass under a uniform vertical magnetic field. Its internal gas volume  $V_g = 0.5$  mL and its ferrofluid volume  $V_{ff} = 15$   $\mu$ L. Picture (a) shows the bubble on a slide when the applied magnetic field intensity  $B_0 = 0$  mT. Image (b) depicts the shape of the bubble under a uniform vertical magnetic field with an intensity of  $B_0 = 11.07$  mT. Picture (c) illustrates the bubble further deformed by an applied field of higher intensity  $B_0 = 41.22$  mT. The size of the bubble meniscus increases with the intensity of the uniform magnetic field. The bubble adopts the shape of a spherical cap sitting atop of a cylinder. The height  $h_b$  and the radius  $R_b$  of the bubble are measured, as well as the meniscus height  $h_m$  and the contact angle at the top of the meniscus  $\theta_b$ .

the magnetic field are equivalent: first the presence of the meniscus in ref. 7 is not due to a soap film, but solely to the magnetic effect (the capillary one being neglected) and second the magnetic field is not uniform and vertical, but circular around the wire. Another configuration closer to ours has, however, been studied by Elias *et al.*:<sup>9</sup> they described the drainage of a flat, vertical film made of ferrofluid soap suspended inside a rectangular frame when submitted to a uniform magnetic field. They notably highlighted the crucial role of the meniscus and the direction of the applied magnetic field on the aforesaid drainage and, in particular, on its velocity. Indeed, a magnetic field applied perpendicularly to the film tends to speed up the drainage, whereas a field applied parallel to the film tends to slow it down. This is due to the interaction between the magnetic moments, which is less (more) favourable inside the film than inside the meniscus when the field is perpendicular (parallel) to the film, thus enhancing (diminishing) the drainage. However, they did not mention any impact on the meniscus shape itself.

As showcased by the different examples presented above, neither the deformations produced by a magnetic field on a droplet or a flat liquid interface, nor those caused in a liquid configuration inducing the presence of a meniscus, can fully explain the observation illustrated in Fig. 2. Our objective is therefore to describe how the unique liquid configuration formed by a bubble and its meniscus deforms under a uniform magnetic field, with particular attention paid to the meniscus since it concentrates most of the deformations.

This paper investigates experimentally this effect and interprets it in terms of an increase in the magnetic pressure inside the bubble meniscus. We show that, conversely to droplets whose shape is prescribed by a magneto/capillary competition, and the Rosensweig's meniscus, described by a magneto/gravity competition, the bubble meniscus is characterised by the interplay between gravity, capillarity and magnetism. Beyond the academic interest of this study, understanding how the bubble deforms and what phenomena drive these changes in shape could help us to better handle bubbles and control their life-span so that they can be used as an actuator in fluid-based systems. In this respect, the experiment presented here can be

seen as complementary to those performed on a bubble under a uniform vertical electric field,<sup>3</sup> as suggested by Fig. 1. Indeed, in the latter case, the deformations are due to a surface force, while in the present case they are due to a volume force. The combination of these two fields could also improve the overall liquid injection induced by electrospray, as carried out on droplets by King *et al.*<sup>22</sup> Finally, as the meniscus grows with the applied magnetic field, measuring the latter is an astute way to directly access the magnetisation in the ferrofluid.

The experimental set-up as well as the method used to study the deformation are presented in Section II. Next, we first explore the overall steady shape of the bubble to determine the magnetic field inside the ferrofluid (Section III). Then, based on dimensional analysis, we propose to rationalise the observation made in Fig. 2 to arrive at a law relating the meniscus height  $h_m$  and the magnetisation inside the ferrofluid  $M$  in the linear magnetisation regime (Section IV). Finally, a general conclusion is drawn in Section V.

## II. Experimental set-up

The deformations due to the application of a uniform magnetic field were studied using two coils mounted in a Helmholtz configuration. The uniformity of the magnetic field between the two coils was verified in a circular area of 50 mm radius whose centre corresponds to that of the coils. The deviation relative to the field at the centre was found to be of the order of 3%, at worst. Moreover, the vertical uniformity of the field was even better, diverging by less than 1% over 20 mm. As the size of the bubbles is smaller, the applied field can be considered uniform over the entire bubble. A power source was used to establish the direct current inside the coils, which was first amplified to reach field intensities of up to 50 mT. The law linking the uniform magnetic field at the centre of the coils to the voltage  $\phi$  used to establish the current was found to be linear as expected. Adjusting this linear law gives us  $B_0 = 6.7\phi - 3$  [mT]. The images of the bubbles were recorded thanks to a camera placed in front of them. To limit their evaporation, the bubbles were caged inside a hermetic chamber made of transparent Perspex sheets with some wadding soaked in water. Sketches of the experimental set-up are presented in Fig. 3.

A droplet of a preset volume of ferrofluid soap  $V_{ff}$  was released onto a horizontal microscope slip glass using a micro pipette with an accuracy of 0.1  $\mu\text{L}$ . After depositing the droplet, a syringe pump was used to inflate the bubble by injecting air directly inside the soapy solution. Bubbles created in this way not only have their size (through the injected air volume  $V_g$ ) fixed, but also the amount of ferrofluid  $V_{ff}$  used to create them. The whole process between the bubble creation and the beginning of the experiment lasted about 10 s. Three initial gas volumes ( $V_g = 1, 0.5$  and  $0.25$  mL) together with five ferrofluid volumes ( $V_{ff} = 3, 7, 15, 30$  and  $60$   $\mu\text{L}$ ) were used. Due to compressibility and air leakage,  $V_g$  could slowly evolve over time, so we therefore determined the precise internal volume *a posteriori*, by imaging, using a classical trapezoidal integration method and taking advantage of cylindrical symmetry.

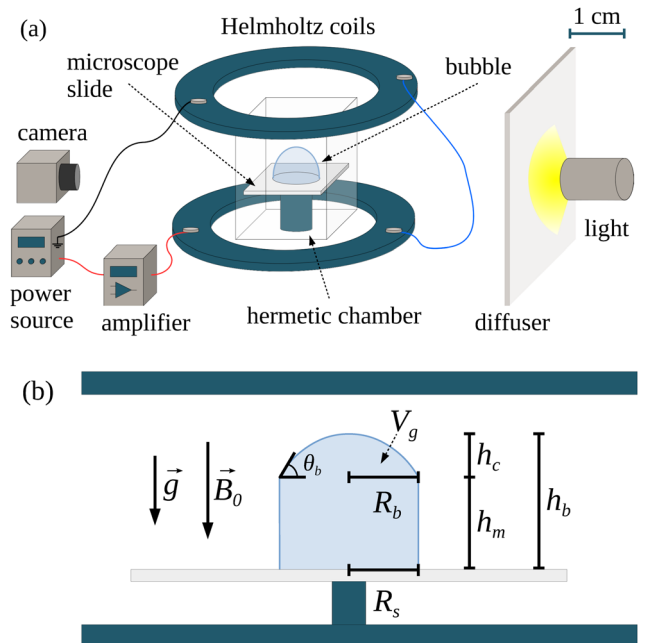


Fig. 3 Sketches of the experimental set-up used for measurements performed on sessile bubbles under a magnetic field. (a) Summary of the elements composing the experimental set-up. (b) Drawing of the geometric measurements of the experiment: the applied magnetic field  $\vec{B}_0$ , the gravity field  $\vec{g}$ , the heights of both the meniscus and the spherical cap forming the bubble ( $h_m$  and  $h_c$  respectively), its total height  $h_b$  and internal volume  $V_g$  as well as the angle at the top of the meniscus  $\theta_b$  and two of its radii  $R_s$  and  $R_b$ . The first, the radius at the slide  $R_s$ , is measured at the contact between the bubble base and substrate, while the second, the common bubble radius  $R_b$ , is taken at the top of the meniscus. The scale of both sketches is roughly the same and is indicated in the upper right-hand corner.

The ferrofluid soap is the same as that used by Elias *et al.*<sup>9</sup> The solution consists of a water-based ferrofluid of maghemite particles ( $\gamma\text{-Fe}_2\text{O}_3$ ) to which 2 wt% of an anionic surfactant, the sodium dodecyl sulfate (SDS), has been added. The physical properties are obtained directly from ref. 9: the surface tension  $\gamma = 30$  mN  $\text{m}^{-1}$  and the density  $\rho = 1.5 \times 10^3$  kg  $\text{m}^{-3}$ . Even if the experimental parameter is the amplitude of the external magnetic field  $B_0$ , the parameter that drives the behaviour of the system is the amplitude of the ferrofluid magnetisation  $M$ . For a ferrofluid, this amplitude is linked to the internal field intensity  $H$  through a magnetisation curve, which is presented in Fig. 4 (obtained with a vibrating sample magnetometer). On this graphic, the blue dots are the measured values and the red curve a phenomenological adjustment of the data with the following function (see ref. 10):

$$M(H) = \frac{\chi_1 M_s H}{M_s + \chi_1 H} \quad (1)$$

where  $\chi_1$  and  $M_s$  are the two fitting parameters,  $\chi_1$  is the magnetic susceptibility in the linear regime and  $M_s$  is the saturation value of the magnetisation. For our ferrofluid soap, the two parameters are equal to  $\chi_1 = 2.65 \pm 0.04$  and  $M_s = 41.00 \pm 0.08$  kA  $\text{m}^{-1}$ .

The experiments were carried out by recording videos in which the intensity of the applied magnetic field  $B_0$  was

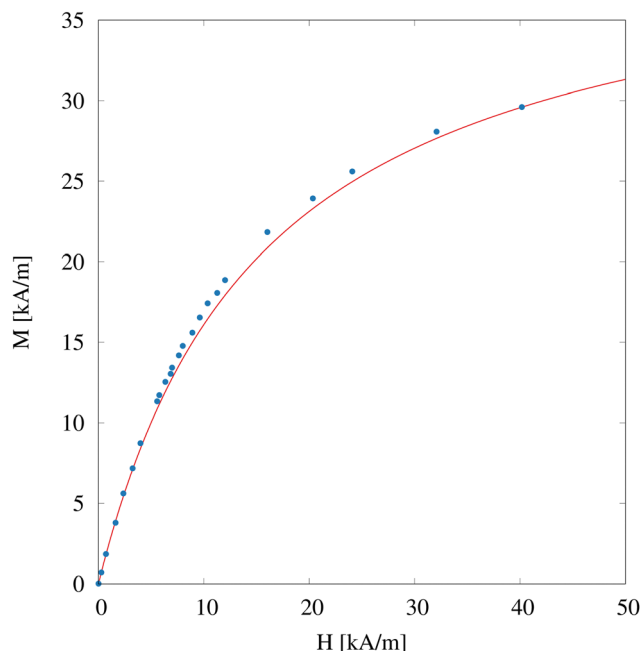


**Fig. 4** The magnetisation curve of the ferrofluid soap obtained using a vibrating sample magnetometer. It represents the amplitude of the ferrofluid magnetisation  $M$  as a function of the field intensity  $H$  inside it. The blue bullets are the measured values, while the red line is the phenomenological adjusted function. This function takes the form described by eqn (1) with  $\chi_1$  and  $M_s$  being the two fitting parameters. For our ferrofluid soap, the fitting parameters are equal to  $\chi_1 = 2.65 \pm 0.04$  and  $M_s = 41.00 \pm 0.08 \text{ kA m}^{-1}$ , respectively.

increased by 2.01 mT every 10 s. The videos are a succession of approximately 5 s of bubble shape recording followed by 5 s of black screen during which the magnetic field is modified, and the bubble reaches its steady shape. As the bubble lifetime did not allow the full range of magnetic fields to be explored (from  $-3 \text{ mT}$  to  $43.23 \text{ mT}$ ), several bubbles were used. Each recording started at  $-3 \text{ mT}$  before either picking up where the last bubble left off or changing the parameters and starting a new sequence. All experiments were performed at least three times and three experiments were done with negative magnetic fields (namely from  $-3 \text{ mT}$  to  $-43.2 \text{ mT}$ ), to verify that only the field intensity mattered and not its direction.

The video recordings from the experiments were cut into constant-field segments and, as the bubble reached a steady regime, each part of the recording was summarised into a single image by averaging all those composing the portion using ImageJ.<sup>23</sup> The average pictures thus obtained were then analysed using a home-made Python code to detect the edge and the meniscus of the bubbles. The various characteristic lengths defining the bubble and meniscus shapes are then extracted, namely the bubble height  $h_b$ , volume  $V_g$  and radii,  $R_s$  and  $R_b$  (measured at the base of the bubble and at the top of the meniscus, respectively), as well as the meniscus and the spherical cap height,  $h_m$  and  $h_c$ . Finally, the angle at the top of the meniscus  $\theta_b$ , is directly measured on the pictures averaged with ImageJ.

The origin of the typical errors on the various geometric lengths (namely  $h_b$ ,  $h_c$ ,  $h_m$ ,  $R_s$  and  $R_b$ ) are all related to the pixels

resolution (which correspond roughly to the pixels size, namely  $30 \mu\text{m}$  in actual length). Since the detection of the bubble's edge, meniscus and base has an accuracy of one or two pixels, the resulting standard error is estimated to be of the order of  $50 \mu\text{m}$  at worst. Moreover, the error on  $V_g$  was determined to be of the order of a few percent and that on  $\theta_b$  to be of the order of  $1^\circ$ . To summarise, this corresponds to a relative error of a few percent or less for all characteristic lengths.

### III. Whole bubbles under magnetic fields

#### A. Meniscus shape

To analyse the deformation of the bubble meniscus, a sessile bubble resting on a microscope cover slip is used (see Fig. 2(a)). In this situation the meniscus height is defined by the surface tension/gravity competition and can be related to the capillary length  $\ell_c = \sqrt{\gamma/\rho g}$ . When we apply a uniform magnetic field, the height of the meniscus increases as the intensity of the applied field does, changing its shape (see Fig. 2(b–c)). Thus, in this second situation, the meniscus shape is a competition between gravity, capillarity and magnetism.

In order to rationalise the effect observed in the pictures presented in Fig. 2, the meniscus height  $h_m$  was measured for an increasing applied field intensity  $H_0$  (where  $B_0 = \mu_0 H_0$  and  $\mu_0$  is the vacuum permeability). The results are presented in Fig. 5 for a bubble of  $V_g = 0.5 \text{ mL}$  and  $V_{\text{ff}} = 15 \mu\text{L}$ . Each point represents the average of three different measurements with

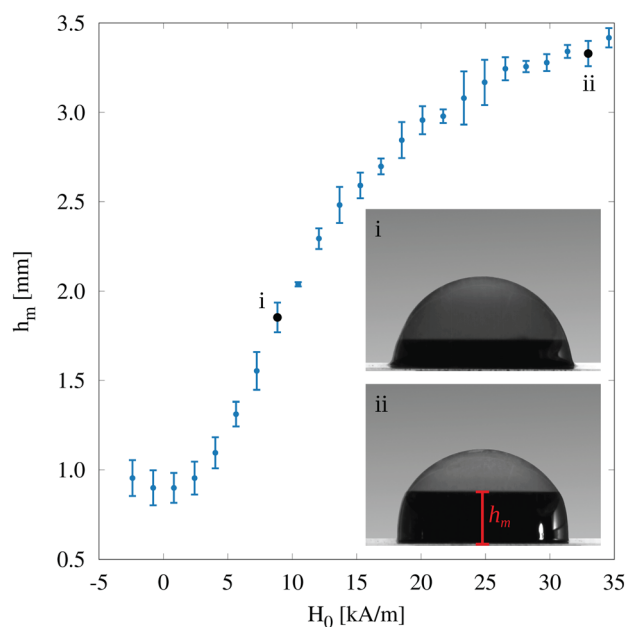


**Fig. 5** Steady height of the bubble meniscus  $h_m$  as a function of the applied field intensity  $H_0$ . The volume of the sessile bubble and the ferrofluid volume used to create it were respectively  $V_g = 0.5 \text{ mL}$  and  $V_{\text{ff}} = 15 \mu\text{L}$ . Each point represents the average of three measurements made on three distinct bubbles, with the associated standard deviation. Picture (i) and (ii) illustrate the bubble shape under  $H_0 = 8.86 \text{ kA m}^{-1}$  and  $H_0 = 32.96 \text{ kA m}^{-1}$  respectively.

the associated standard deviation. Pictures (i) and (ii) of Fig. 5 show the ferrofluid bubble under a field intensity  $H_0 = 8.86 \text{ kA m}^{-1}$  and  $H_0 = 32.96 \text{ kA m}^{-1}$  respectively (corresponding to  $B_0 = 11.07 \text{ mT}$  in Fig. 2(b) and to  $B_0 = 41.22 \text{ mT}$  in Fig. 2(c)). A first observation can be made: as the applied field intensity  $H_0$  increases and the meniscus rises, the shape of the sessile bubble changes from a hemispherical shape to one that closely resembles that of a spherical cap sitting atop of a cylinder, with the meniscus forming the cylinder.

This effect is due to the internal field  $\vec{H}$  inside the meniscus which, in general, depends on the overall shape of the bubble through the demagnetising factor  $D$ . This demagnetising factor and the corresponding field  $\vec{DM}$  arise from the magnetic dipole interaction inside the ferrofluid which lowers the internal field  $\vec{H}$ . This effect can be expressed as follows

$$\vec{H} = \vec{H}_0 - \vec{DM}. \quad (2)$$

Since most of the ferrofluid is concentrated inside the meniscus, which is very similar in shape to a cylinder, we have assumed that the ferrofluid forms a cylinder with a thickness  $e_m$ . To validate the cylinder hypothesis, the radius at the base of the bubble and that at the top of the meniscus, respectively labelled  $R_s$  and  $R_b$ , were measured. The closer the values of the radii are, the more valid the hypothesis is. The results are presented in Fig. 6 for the different values of  $V_{\text{ff}}$  and  $V_g$  as well as for all field intensity  $H_0$ . It can be observed that the radii are close to each other even though the base radius  $R_s$  is always a bit larger than that taken at the top of the meniscus  $R_b$ . Yet, the difference between the radii is small compared with the values of the radii, so the cylinder hypothesis gives a fairly good description of the situation.

## B. Cylindrical hypothesis

In order to refine the cylindrical hypothesis, variation of the radii was measured as a function of the applied field intensity  $H_0$ . The results show that for small amounts of ferrofluid, the radii remain independent of  $H_0$ , whereas, for larger quantities, the meniscus shrinks as  $H_0$  increases. This shrinkage is due to the finite value of  $V_{\text{ff}}$  and the need to fuel  $h_m$  growth and is associated with the values of  $R_b$  and  $R_s$  approaching each other. Consequently, as the field intensity  $H_0$  and the meniscus height  $h_m$  increase, the shape of the meniscus becomes increasingly similar to that of a cylinder.

Together, the information gathered from the radii analysis allows us to conclude that the difference between the radii is small compared to the value of  $h_m$ , except for low values of the applied field  $\vec{H}_0$  where they can be comparable. Under these conditions, the ferrofluid can be considered to rise almost perpendicularly to the substrate, forming a cylinder. The radius of this cylinder is assumed to be equal to the average of the two radii, namely  $R_a = (R_b + R_s)/2$ , its height equal to  $h_m$  and its volume to  $V_{\text{ff}}$ . Indeed, the quantity of liquid inside the spherical cap  $V_c$  is approximately equal to  $2\pi R_a^2 e_c$ , where  $e_c$  is the film thickness (assuming a hemispherical shape for the cap, which is the upper limit). Taking  $e_c \approx 1 \mu\text{m}$  and  $R_a \approx 5 \text{ mm}$ ,  $V_c < 0.2 \mu\text{L}$  which is, at least, an order of magnitude smaller than  $V_{\text{ff}}$ .

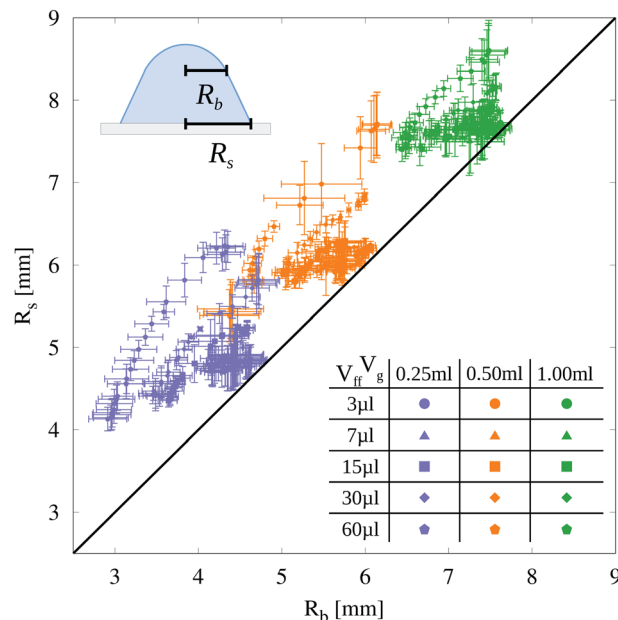


Fig. 6 Values of  $R_s$  as a function of  $R_b$  for all applied fields intensity  $H_0$ , the five ferrofluid volumes  $V_{\text{ff}}$  considered and the three air volumes used  $V_g$ :  $V_{\text{ff}} = 3 \mu\text{L}$  represented by solid circles,  $V_{\text{ff}} = 7 \mu\text{L}$  by solid triangles,  $V_{\text{ff}} = 15 \mu\text{L}$  by solid squares,  $V_{\text{ff}} = 30 \mu\text{L}$  by solid diamonds and  $V_{\text{ff}} = 60 \mu\text{L}$  by solid pentagons together with  $V_g = 0.25 \text{ mL}$  in lilac,  $V_g = 0.50 \text{ mL}$  in orange and  $V_g = 1.00 \text{ mL}$  in green. Each point represents the average of three measurements with the corresponding standard deviations and the black line is a guide representing  $R_b = R_s$ . The difference between the two radii has been exaggerated on the sketch displaying  $R_s$  and  $R_b$ .

Finally, we can estimate that the cylinder thickness  $e_m$  is equal to  $V_{\text{ff}}/2\pi R_a h_m$  and calculate the ratio  $e_m/R_a$ . The latter ranges from  $3 \times 10^{-3}$  in the best-case scenario, to 0.13 in the worst one. The worst-case scenario corresponds to  $V_g = 0.25 \text{ mL}$ ,  $V_{\text{ff}} = 60 \mu\text{L}$  and weak applied fields  $\vec{H}_0$ . Considering these values and since the approximation improves with increasing field strength, it is realistic to assume that the meniscus has a cylindrical shape with a thickness at least ten times smaller than its radius for all sets of parameters.

The demagnetising factor corresponding to a thin cylindrical shell submitted to an external magnetic field parallel to the cylindrical axis was derived by Beleggia *et al.*<sup>24</sup> Given the obtained thickness over the radius ratio, this leads to a  $D$  ranging from  $\approx 0.01$  to  $\approx 0.1$ . Consequently, since  $M$  is of the same order of magnitude as  $H$ , the demagnetising field can be neglected. Hence, the effects of the dipolar magnetic interactions can be ignored in our experiments and the internal field in the ferrofluid hollow cylinder  $\vec{H}$  is equal to the external applied field  $\vec{H}_0$ . This approximation is especially accurate for large  $\vec{H}_0$  and small  $V_{\text{ff}}/V_g$  ratios. Even in the least favourable cases, deviations from the model should be small taking the upper limit of  $D$  into account.

## C. Bubble cap

Above the meniscus, the thin film of soap that closes the bubble is almost transparent and can therefore be assumed to contain a very small amount of ferrofluid, as estimated above. Therefore, both effects of  $H_0$  and gravity are assumed to be negligible,

and the film should take a shape prescribed by surface tension alone, namely a spherical cap. To validate this hypothesis, the measured spherical cap height  $h_{c,m}$  can be compared with the calculated one  $h_{c,c}$ . These are obtained from the measured cylinder radius  $R_a$  and the angle measured at the top of the meniscus  $\theta_b$ . Assuming a spherical cap, this leads to

$$h_{c,c} = R_a \frac{1 - \cos(\theta_b)}{\sin(\theta_b)}. \quad (3)$$

The closer these two values (*i.e.*  $h_{c,m}$  and  $h_{c,c}$ ) are, the less effect gravity and magnetism have on the soap film.

In Fig. 7 each point once again represents the average of three measurements with the corresponding standard deviation. The measured and calculated  $h_c$  are plotted for each set of parameters, namely for the five  $V_{ff}$ , the three  $V_g$  and for all applied fields intensity  $H_0$ . The solid black line is a guide for the eyes representing  $h_{m,c} = h_{c,c}$ . As can be seen, if the standard deviation is taken into account, all the data indicate that the calculated and measured heights are equal. Consequently, in the following, we consider that the part of the bubble located at the top of the meniscus adopts a spherical cap shape.

## IV. Model

### A. Meniscus under magnetic fields

According to Rosensweig<sup>7</sup> the influence of the magnetic field on the ferrofluid can be described by three distinct pressures.

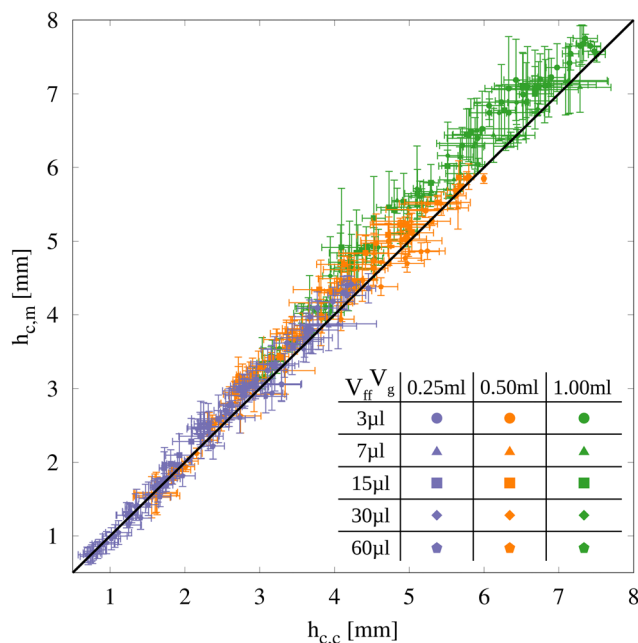


Fig. 7 Comparison between the calculated height  $h_{c,c}$  and the measured height  $h_{c,m}$  for each set of parameters  $V_g$ ,  $V_{ff}$  and for all applied fields intensity  $H_0$ . The three air volumes  $V_g$  and the five ferrofluid volumes  $V_{ff}$  used are represented in the same fashion as in Fig. 6:  $V_g = 0.25$  mL in lilac,  $V_g = 0.50$  mL in orange and  $V_g = 1.00$  mL in green together with  $V_{ff} = 3$   $\mu$ L with solid circles,  $V_{ff} = 7$   $\mu$ L with solid triangles,  $V_{ff} = 15$   $\mu$ L with solid squares,  $V_{ff} = 30$   $\mu$ L with solid diamonds and  $V_{ff} = 60$   $\mu$ L with solid pentagons. The black line is a guide that represents  $h_{c,c} = h_{c,m}$ .

The first is the pressure linked to the magnetostrictive effects  $P_s$ , which is, in our case, assumed to be null since the ferrofluid density is seen as independent of the magnetic field. The second is the magnetic overpressure inside the fluid due to the interaction between the magnetic moments  $P_m$ . Finally, the third is the pressure due to the magnetisation perpendicular to the interface  $P_n$ . This last term is also assumed to be zero because the magnetisation due to the applied field is parallel to the liquid–air interface of the hollow ferrofluid cylinder. Consequently, the pressure equilibrium inside the ferrofluid under a field intensity  $H$  can be obtained by combining a generalised Pascal's principle and the associated boundary conditions. The expression thus obtained is constant everywhere inside the fluid for an imposed field intensity  $H$  and reads as follows

$$P_0 + P_\gamma - \mu_0 \int_0^H M dH^* + \rho g z = \text{cst}, \quad (4)$$

where  $P_0$  and  $P_\gamma$  are respectively the atmospheric and capillary pressures,  $z$  is the liquid height and  $M$  is its magnetisation. The third term of the equation is the expression for the in-fluid magnetic pressure  $P_m$ . This equation is applicable everywhere inside the ferrofluid forming the bubbles and therefore inside the whole meniscus. Yet, it cannot be used to directly predict the effect of a change in  $\vec{H}$  as the constant depends on the field, otherwise nothing would vary. To circumvent this difficulty, we propose to use dimensional analysis to rationalise our observations.

Assuming that the bubble is large enough that its horizontal curvature has no influence, the meniscus shape can be entirely characterised by its height  $h_m$ . Moreover, according to eqn (4), the pressures involved in its creation are the hydrostatic, capillary and magnetic pressures respectively described by  $P_h \sim \rho g h_m$ ,  $P_\gamma \sim \gamma h_m^{-1}$  and  $P_m$ . As the magnetisation  $M$  is related to the internal field intensity  $H$  by eqn (1), the set of magnetic effects can be characterised by two dimensional parameters  $M$  and  $\mu_0$  and a dimensionless one  $\chi$ , the magnetic susceptibility. We have chosen to keep  $M$  instead of  $H$  or  $H_0$  because  $M$  is related to the magnetic effects inside the ferrofluid. Consequently, the height  $h_m$  can be defined as a function of five dimensional parameters,  $\rho$ ,  $g$ ,  $\gamma$ ,  $\mu_0$  and  $M$  and a dimensionless one  $\chi$ . Four of the dimensional parameters have independent dimensions and the dimension of the fifth can therefore be expressed as a product of the others. If the dimension of  $\mu_0$  is chosen as the dependent one, it can be formulated as follows

$$[\mu_0] = [\rho]^{1/2} [g]^{1/2} [\gamma]^{1/2} [M]^{-2}. \quad (5)$$

Moreover, the dimension of  $h_m$  is also expressed as the product of the same four dimensional parameters:

$$[h_m] = [\rho]^{-1/2} [g]^{-1/2} [\gamma]^{1/2} [M]^0. \quad (6)$$

Then, according to the dimensional analysis and the Buckingham  $\Pi$ -theorem,<sup>25</sup> the following relationship applies:

$$h_m = \ell_{cfm} \left( \frac{\mu_0 M^2}{\sqrt{\rho g \gamma}}, \chi \right) \quad (7)$$

where  $f_m(\mu_0 M^2 / \sqrt{\rho g \gamma}, \chi)$  is a function of the two dimensionless

numbers  $\mu_0 M^2 / \sqrt{\rho g \gamma}$  and  $\chi$  and  $\ell_c = \sqrt{\gamma / \rho g}$  is the capillary length.

The expression of  $h_m$  can be manipulated to highlight the two characteristic lengths of the problem. If we define the magnetic length  $\ell_m$ :

$$\ell_m = \frac{\mu_0 M^2}{\rho g}, \quad (8)$$

Eqn (7) can be rewritten as a function of  $\ell_c$  and  $\ell_m$ :

$$h_m = \ell_c f_m \left( \frac{\ell_m}{\ell_c}, \chi \right). \quad (9)$$

The two characteristic lengths reflect a competition between a driving effect, which pulls the liquid upwards, and a restraining effect, which has the opposite outcome. For both characteristic lengths, the restraint is gravity, which pulls the ferrofluid down, but the motor is different. In  $\ell_c$ , it is capillarity that is at work, whereas in  $\ell_m$  it is the magnetic in-fluid pressure  $P_m$ . As  $f_m$  is a function of the ratio between these two lengths, two different regimes are expected: one dominated by capillarity and the other by magnetic pressure. The transition between these two regimes occurs when the two lengths are equal, namely at a critical magnetic field  $M_c \approx 4.2 \text{ kA m}^{-1}$ . In the capillary regime, the meniscus shape is close to the usual one (see Fig. 2(a)). In the magnetic regime, the meniscus shape is gradually transformed into a cylinder. This metamorphosis erases the initial curvature of the meniscus, inducing the disappearance of the capillary pressure associated to this curvature. As the horizontal curvature is not taken into account in this first-order model, capillarity and magnetism can be considered to act solely in their respective regimes.

To highlight the effect of the magnetic field on the meniscus height,  $h_m$  was plotted as a function of the squared amplitude of the magnetisation  $M^2$  in Fig. 8 for each volume of air ( $V_g = 1, 0.5$  and  $0.25 \text{ mL}$ ) and volume of ferrofluid ( $V_{ff} = 3, 7, 15, 30$  and  $60 \mu\text{L}$ ). The labels used in the figure are the same as previously and each point represents the average of three different measurements with the corresponding standard deviation. The vertical red line indicates the transition between the capillary-dominant ( $M < M_c$ ) and magnetic-dominant regimes ( $M \geq M_c$ ). As can be seen, only the points corresponding to a very weak magnetic field belong to the first regime (the first two points of each data set, corresponding to a negative value of  $M$ , have been omitted from this graph for clarity). Therefore, almost the entire range of applied fields corresponds to a meniscus shape prescribed by the magnetic field. Another observation can be made on this graphic: all data seem to be roughly sorted into five categories, each corresponding to a different  $V_{ff}$ . Furthermore,  $h_m$  appears to linearly depend on  $M^2$  as long as the intensity of the field is weak (*i.e.* for  $M \leq 21 \text{ kA m}^{-1}$ , which is nearly half of the data range). Consequently, a linear expression for  $f_m$  in the weak field limit can be proposed.

### B. Meniscus: linear regime

For very weak fields, in the capillary regime ( $M < M_c$ ),  $h_m$  is directly linked to the capillary length  $\ell_c$ , which expresses the

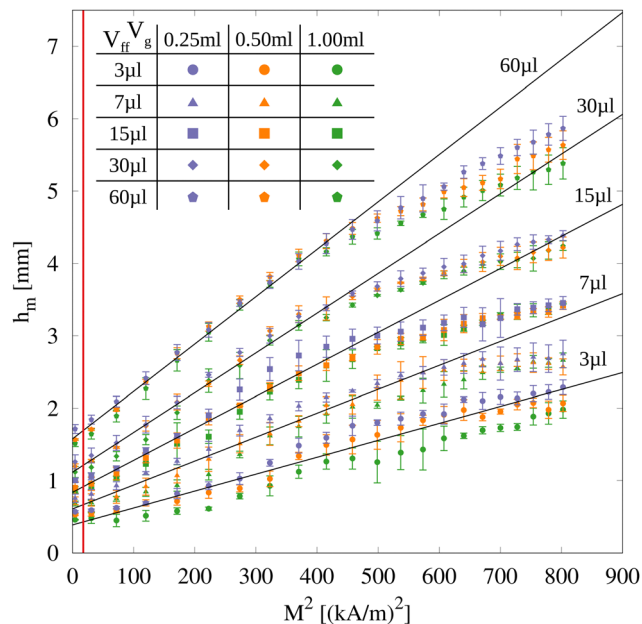


**Fig. 8** Height of the meniscus  $h_m$  drawn as a function of the squared amplitude of the magnetisation  $M^2$  for each volume of air ( $V_g = 1, 0.5$  and  $0.25 \text{ mL}$ ) and ferrofluid volume ( $V_{ff} = 3, 7, 15, 30$  and  $60 \mu\text{L}$ ). The label used is the same as in the previous figure and, similarly, each point represents the average of three measurements with the corresponding standard deviation. The vertical red line marks the separation between the capillary-dominant regime and the magnetic-dominant one, namely when  $M_c^2 = 17.64 \text{ kA m}^{-1}$ . The black lines, corresponding to each  $V_{ff}$ , are the functions that describe the meniscus growth in the linear regime. They are obtained thanks to the mean slope represented in Fig. 10 and the average of the three heights in the capillary regime  $h_{m,0}$  displayed in Fig. 9.

opposition between  $P_\gamma$  and  $P_h$ . In particular, for a floating bubble subjected to no field other than gravity, Teixeira *et al.*<sup>2</sup> proposed an expression for  $h_m$ . Moreover, a method similar to that used to determine the height of the meniscus formed by a liquid bath along a solid wall (see ref. 26 pages 48–50 for example) can be used for those that are sessile. However, the latter configuration is quite different from our case (there is no solid on which to wet and a finite amount of ferrofluid) and the result can therefore only be considered as an estimate. Nevertheless, in both cases,  $h_m$  can be expressed as  $h_m = C_1 \ell_c$ , with  $C_1$  a constant that depends on the bubble size in the floating bubble case and on the contact angle in the solid wall situation. Dimensional analysis leads to exactly the same result for our configuration under a null magnetic field with  $C_1$  depending on both  $V_g$  and  $V_{ff}$  (see the zero-field values of  $h_m$  in Fig. 8).

In the magnetic regime ( $M \geq M_c$ ), the meniscus height is determined by  $\ell_m$ , which reflects the competition between  $P_m$  and  $P_h$ . Rethinking the dimensional analysis in this regime, namely without the capillary pressure influence, leads us to  $h_m = f(\chi) \ell_m$ , where  $f(\chi)$  is a function of the magnetic susceptibility. In addition, according to eqn (1), when the field inside the liquid is weak compared with the saturation magnetisation  $M_s$ , the magnetisation is a linear function of the field, namely  $M(H) \approx \chi_1 H$ . Under these conditions, the internal magnetic pressure  $P_m$  takes a much simpler form:  $P_m \sim \mu_0 M^2 / 2 \chi_1$ . This

linear regime can define a weak field limit  $M_1 = 21 \text{ kA m}^{-1}$ , the value at which  $h_m$  stops increasing linearly with  $\ell_m$ . Therefore, in the weak field limit, namely when  $M \leq M_1$ , equating  $P_m$  and  $P_h$  gives us the characteristic height of the meniscus, which is equivalent to  $\ell_m/2\chi_1$ . Therefore, since  $\chi_1$  is constant and taking into account the dimensional analysis in the magnetic regime, the height of the meniscus under a weak field can be expressed as  $h_m = (C_2/2\chi_1)\ell_m$ , with  $C_2$  a constant.

Accordingly, assuming that capillary and magnetic pressures only act in their respective regimes, a function that satisfies the definition given by eqn (9) can be proposed under the weak field limit. On one hand, the meniscus height in the capillary regime is  $h_{m,0} = C_1\ell_c$ , which is independent of the magnetisation. On the other hand, in the weak field regime,  $h_m$  grows linearly with  $\ell_m$ . By combining the results obtained in both regimes, the meniscus height can be expressed as

$$h_m = \begin{cases} h_{m,0}, & \text{if } M \in [0, M_c] \\ h_{m,0} + C_2 \frac{\Delta\ell_m}{2\chi_1}, & \text{if } M \in [M_c, M_1] \end{cases} \quad (10)$$

where  $h_{m,0} = C_1\ell_c$  is the meniscus height in the capillary regime and  $\Delta\ell_m = \ell_m(M) - \ell_m(M_c)$ . In addition, the data represented in Fig. 8 indicate that  $h_{m,0}$  vary drastically with  $V_{ff}$  and, to a lesser extent, with  $V_g$ .

### C. Experimental validation

To ensure the validity of the first-order model, the linear part of eqn (10) can be adjusted to each data set represented in Fig. 8. Fitting the function over the weak field domain, namely for  $M \in [M_c, M_1]$ , allows us to obtain both  $h_{m,0}$  and  $C_2$ . The dependencies of the first of these two parameters can be further rationalised. Indeed, the dimensional analysis in the capillary regime states that  $h_{m,0}$  is proportional to the capillary length  $\ell_c$ , but the observation made in Fig. 8 shows that  $h_{m,0}$  also depends on both  $V_{ff}$  and  $V_g$ . This second variation in  $V_{ff}$  and  $V_g$  is the sign of the influence of the finite amount of ferrofluid used to create the bubble.

To explore this dependence, we assume that the meniscus has a height  $h_{m,0}$  of the same order of magnitude as its lateral extension, *i.e.* that it has a constant curvature, and that its shape is the same inside and outside the bubble. These assumptions make it symmetrical with respect to the plane perpendicular to the substrate and passing through its middle. Under these conditions, geometric arguments and cylindrical symmetry allow us to link  $V_{ff}$  and  $h_{m,0}$  using the following formula

$$h_{m,0}^2 = C_s \frac{V_{ff}}{R_0} \quad (11)$$

where  $C_s$  is a shape constant and  $R_0$  is the radius of the bubble in the capillary-dominant regime, which is proportional to  $\sqrt[3]{V_g}$  due to the bubble hemispherical shape. This radius is defined in the same way as for the cylinder, by taking an average of the base radius  $R_s$  and the radius at the top of the meniscus  $R_b$ . The graphic of  $h_{m,0}^2$  as a function of  $V_{ff}/R_0$  is presented in Fig. 9. The data points are obtained by adjusting a linear function to the

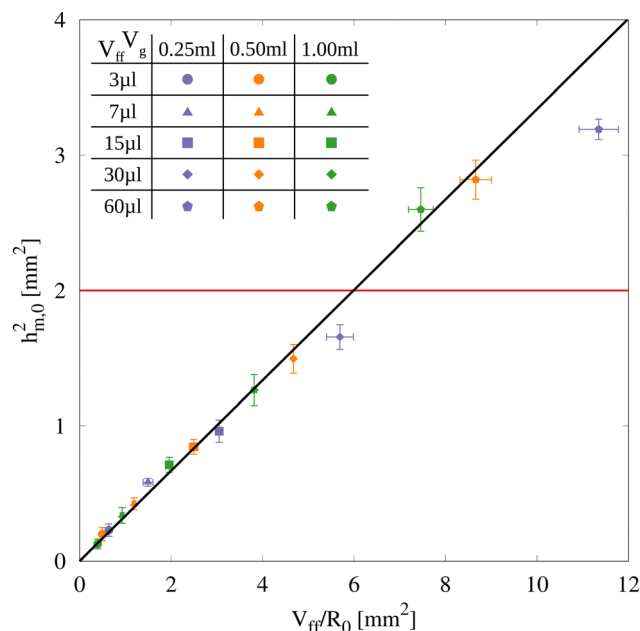
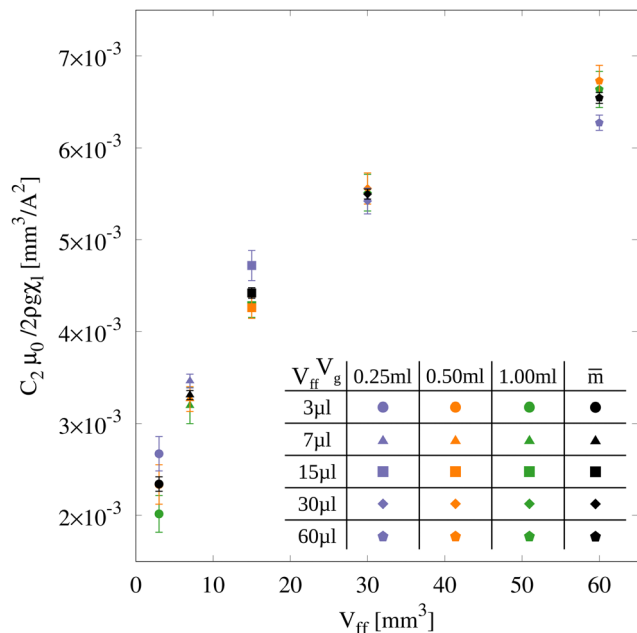


Fig. 9 Initial meniscus height squared  $h_{m,0}^2$  which is the square of the first fitting parameter obtained by adjusting the linear part of the function defined in eqn (10) on each set of parameters. This height is plotted as a function of  $V_{ff}/R_0$  and each point is displayed with the label corresponding to its data set. The vertical standard deviation is obtained from that given by the fitting procedure and the horizontal one is based on the error on  $R_0$ . The black line is the law obtained by adjusting eqn (11) to the  $h_{m,0}^2$  smaller than the square of the capillary length, represented by the red line, and the fitting procedure gives  $C_s = 0.33 \pm 0.01$  (the standard deviation is given by the adjustment procedure).

meniscus height values corresponding to the linear regime of magnetisation. The points relative to each data set are shown with the corresponding label. The vertical standard deviation is calculated by propagating that given by the adjustment procedure. Furthermore, to determine the horizontal standard deviation, we have considered that the error on the pipetted volume of ferrofluid is small enough to be neglected and the error is therefore based on that on  $R_0$ .

The black line is an adjustment of eqn (11) with  $C_s$  taken as the only fitting parameter. Moreover, only the data corresponding to  $h_{m,0}^2 < \ell_c^2$  were used to adjust the function. Indeed, eqn (11) describes the influence of the finite amount of ferrofluid  $V_{ff}/R_0$ , but does not take the potential influence of  $\ell_c$  into account. Yet, when the meniscus height becomes comparable to the capillary length, we expect gravity to start limiting  $h_{m,0}$ . The data is therefore separated into two categories: in the first  $h_{m,0}$  it is only limited by  $V_{ff}/R_0$  and described by eqn (11) while, in the second,  $h_{m,0}$  results from both  $\ell_c$  and the available ferrofluid quantity  $V_{ff}/R_0$ . The separation between the regimes is represented by the horizontal red line. The obtained value for the shape constant  $C_s = 0.33$  is close to that obtained by assuming a constant curvature (in this case  $C_s = (\pi(4 - \pi))^{-1} \approx 0.37$ ). As can be seen, the evolution of  $h_{m,0}$  is fairly well described by eqn (11), except maybe for the higher values of  $V_{ff}/R_0$ , where it starts to diverge from the prediction. For these large  $V_{ff}/R_0$  values, we observe that the lateral extension of the meniscus



**Fig. 10** Slopes of the adjusted function  $C_2\mu_0/2\rho g\chi_1$  defined by eqn (10) as a function of  $V_{ff}$ . Each point represents the value obtained for a given data set and is displayed with the same label. Standard deviations are given by the adjusting procedure. The black bullets represent the mean values for each  $V_{ff}$  obtained by fitting a linear law defined by eqn (12) on all  $\Delta h_m$  corresponding to a given  $V_{ff}$ . Here again, the standard deviations are given by the adjusting procedure.

starts to become larger than its height, which is surely the reason for this discrepancy.

According to eqn (10), the slope of the weak magnetic field function is equal to  $C_2\mu_0/2\rho g\chi_1$ . This slope has been plotted as a function of  $V_{ff}$  in Fig. 10, labelled in the same way as in the previous figure. Again, the vertical standard deviation comes from the adjusting procedure. As shown, the slopes are a function of  $V_{ff}$ , but appear to be almost independent of  $V_g$  when the error bars are considered. The values of  $C_2$  can be evaluated knowing that  $\mu_0/2\rho g\chi_1 \approx 1.6 \cdot 10^{-2} \text{ mm}^3 \text{ A}^{-2}$ . This gives us a value of  $C_2 = 0.146$  for  $V_{ff} = 3 \mu\text{L}$  to  $C_2 = 0.409$  for  $V_{ff} = 60 \mu\text{L}$ . Since  $C_2$  is independent of  $V_g$ , global values of the slopes can be used for each  $V_{ff}$ . These average slopes were obtained by adjusting a single linear function to all points corresponding to a given  $V_{ff}$  (black bullets in Fig. 10). Furthermore, it should be noted that Fig. 9 and 10 suggest that  $h_{m,0}$  and  $C_2$  could reach saturation values for sufficiently large  $V_{ff}$ . These saturation values could be obtained by using floating bubbles, although in this case there may be a non-negligible effect of the demagnetising field at the surface of the liquid bath, which in turn may induce internal field gradients as observed in ref. 9. Nevertheless, this work is beyond the scope of the experimental study presented here. Finally, since  $\chi_1$  contains all the information about the specificities of the ferrofluid, both  $h_{m,0}$  and  $C_2$  can be presumed to be universal and therefore do not depend on the ferrofluid used.

In order to highlight the evolution of  $h_m$  in the magnetic regime ( $M \geq M_c$ ), eqn (10) can be rewritten to express the

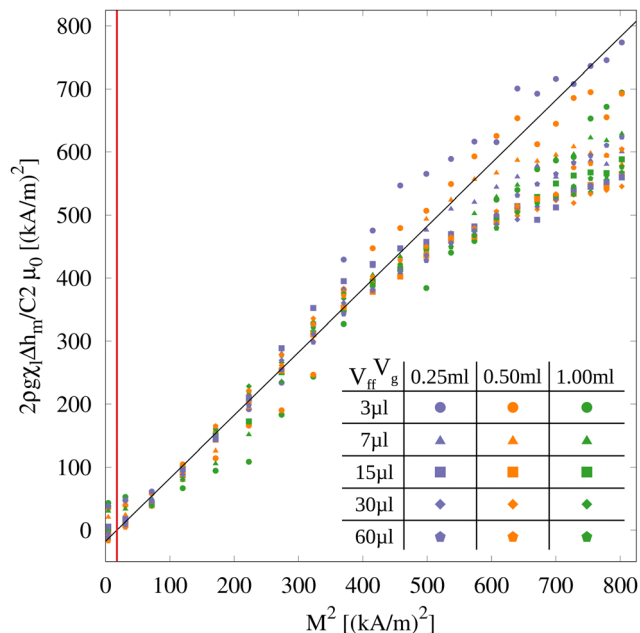


**Fig. 11** Variation of the meniscus height  $\Delta h_m$  divided by the slope of the linear law  $C_2\mu_0/2\rho g\chi_1$  corresponding to a given  $V_{ff}$  as a function of  $M^2$  for all the parameters. The labels used are the same as in the previous graphics and each point corresponds to the average of three measurements for a given  $V_g$  and  $V_{ff}$ . The red line marks the transition between the capillary-dominant and the magnetic-dominant regimes. The standard deviations have been omitted to maintain a readable representation. Their order of magnitude is the same as in Fig. 8 (more precisely, the error bars are slightly larger due to errors in  $h_{m,0}$  and  $C_2$ ). Finally, the black line is a guide representing  $2\rho g\chi_1\Delta h_m/C_2\mu_0 = (M - M_c)^2$ .

variation of the meniscus height  $\Delta h_m = h_m - h_{m,0}$  as a function of  $M^2$ . Accordingly,  $\Delta h_m$  is described by the following law:

$$\Delta h_m = C_2 \frac{\Delta \ell_m}{2\chi_1}, \quad (12)$$

with  $C_2$  as the only fitting parameter and, since  $h_{m,0}$  contains all the dependence in  $V_g$ , with  $\Delta h_m$  a function of  $\ell_m$  and  $V_{ff}$ . Therefore, if  $\Delta h_m$  is divided by the slope corresponding to its given  $V_{ff}$ , the resulting measure  $2\rho g\chi_1\Delta h_m/C_2\mu_0$ , which has the unity of a squared magnetisation, depends only on  $\ell_m$ .

This result is presented as a function of  $M^2$  in Fig. 11. The representations used in this figure are the same as those in Fig. 8 except that the standard deviations are not shown for clarity. The black line is a guide representing  $2\rho g\chi_1\Delta h_m/C_2\mu_0 = (M - M_c)^2$ . On this graphic, we see that the data do indeed collapse on a master curve, not only in the weak field regime, but also beyond. The existence of this master curve validates the dimensional analysis and confirms that  $h_m$  is described by eqn (9). Thanks to this master curve, the magnetisation value at which the data ceases to be correctly grasped by the linear approximation can be corroborated. It appears that the linear law is meaningful over half of the data range (namely for  $M \leq M_1 = 21 \text{ kA m}^{-1}$ ). After the linear regime, the deformations saturate as expected from the magnetisation curve.

## V. Conclusion

The experiments presented here as well as their description confirm that, as presumed in the introduction, the interplay between the intrinsically volumetric nature of the magnetic force and the unique ferrofluid distribution inside a bubble is responsible for its singular behaviour and deformation. Indeed, for example, when comparing bubbles to droplets under the same conditions, there is not only a clear distinction between their shape, but also in the location and expression of the magnetic effect.<sup>17</sup> Unlike droplets where capillarity and magnetism counteract each other, in bubbles, both capillarity and magnetism favour meniscus growth, as showcased by the two characteristic lengths of the phenomenon: the capillary length  $\ell_c$  and the magnetic length  $\ell_m$ . These two lengths appear as a ratio in eqn (9) and the growth of the meniscus is therefore driven by two distinct regimes: a capillary and a magnetic one. In the first regime,  $h_{m,0}$  is determined by  $V_{ff}/R_0$  (see eqn (11)) when the amount of ferrofluid is small and by a combination of  $V_{ff}/R_0$  and  $\ell_c$ , when there is enough ferrofluid (see Fig. 9). In the second regime, the shape assumed by the meniscus is a cylinder due to the competition between the alignment of the magnetic dipoles with the internal field and gravity. In particular, the meniscus height under weak fields (*i.e.* for  $M < 21 \text{ kA m}^{-1}$ ) evolves linearly with the square of the magnetisation and is represented by eqn (10). Moreover, the slope in the linear regime only depends on  $V_{ff}$  (see Fig. 10) and a master curve expressing the meniscus growth as a function of  $\ell_m$  can be obtained by dividing the  $\Delta h_m$  by their corresponding slope (see Fig. 11). Finally, conversely to drops under the magnetic field, we did not observe a critical magnetic field at which the bubble blew up and the ferrofluid volume separates into several daughter droplets.

The volumetric nature of the magnetic force can be further highlighted by comparing the deformation induced by an electric or magnetic field on a bubble (see Fig. 1). Indeed, although they both influence the liquid phase of the bubbles, they clearly do not deform the bubble in the same way. Due to its superficial nature, the electric force mainly affects the liquid distribution with the largest surface-to-volume ratio, namely the liquid shell, deforming into a hemispherical shell under weak fields and into a Taylor cone beyond a critical one. Conversely, the volumetric nature of the magnetic force induces effects within the liquid distribution with the smallest surface-to-volume ratio, *i.e.* the meniscus.

The study presented here sheds new light on the interplay between gravity, capillary and magnetic effects thanks to the bubble unique liquid configuration. Our analysis allows for a better grasp of how to handle, control and especially deform a bubble using external fields. In this respect, it can be considered complementary to the work done on bubbles under electric fields.<sup>3</sup> Yet, these results constitute a first step and also raise unresolved questions. Firstly, studying this system at very low fields or with ferrofluids having lower  $\chi_1$  could highlight the transition between the capillary and the magnetic regimes and allow us to explore how the shape of the meniscus changes when determined by gravity, capillarity and magnetism together.

Secondly, other ferrofluid soaps can be used to probe the influence of  $\chi$ , the second dimensionless number presented in eqn (9). Thirdly, although the weak field limit  $M_1$  is certainly linked to the saturation of the magnetisation curve, further investigation of its physical meaning could help propose a law based on the whole magnetisation curve and to identify whether this limit is universal or not. Finally, submitting bubbles floating on their own ferrofluid to a magnetic field could help us complete the picture drawn in this paper. This presumption is based on Fig. 9 and 10, which suggest that the values of  $h_{m,0}$  and  $C_2$  could reach saturation for an infinite amount of liquid. Floating bubbles therefore seem perfectly suited to obtain these values and get rid of the influence on the limited volume of ferrofluid available to make the bubble.

## Conflicts of interest

There are no conflicts to declare.

## Acknowledgements

S. M. thanks Eric Falcon for the loan of part of the experimental set-up, Charlotte Marique for her careful reading and Florence Mignolet for her wise advice as well as her attentive reading. S. D. thanks F. R. S.-FNRS for its financial support as Senior Research Associate. F. E. thanks Cyprien Gay for the fruitful discussions and Delphine Talbot for the magnetisation curve.

## References

- 1 C. Cohen, B. D. Texier, E. Reyssat, J. H. Snoeijer, D. Quéré and C. Clanet, On the Shape of Giant Soap Bubbles, *Proc. Natl. Acad. Sci. U. S. A.*, 2017, **114**, 2515.
- 2 M. A. C. Teixeira, S. Arscott, S. J. Cox and P. I. C. Teixeira, What is the Shape of an Air Bubble on a Liquid Surface?, *Langmuir*, 2015, **31**, 13708.
- 3 S. Mawet, H. Caps and S. Dorbolo, Deformation of soap bubbles in uniform electric fields, *Phys. Rev. Fluids*, 2021, **6**, 043603.
- 4 W. A. Macky, Deformation of Soap Bubbles in Electric Fields, *Math. Proc. Camb. Philos. Soc.*, 1930, **26**, 421.
- 5 C. T. R. Wilson and G. I. Taylor, The Bursting of Soap-bubbles in a Uniform Electric Field, *Math. Proc. Camb. Philos. Soc.*, 1925, **22**, 728.
- 6 S. S. Papell, *Inventor; NASA (United States of America), assignee. Low viscosity magnetic fluid obtained by colloidal suspension of magnetic particles, US Pat.*, 3215572, 1965.
- 7 R. E. Rosensweig, *Ferrohydrodynamics*, Dover Publications, New York, United States, 2014.
- 8 J. C. Bacri, R. Perzynski, D. Salin, V. Cabuil and R. Massart, Phase diagram of an ionic magnetic colloid: Experimental study of the effect of ionic strength, *J. Colloid Interface Sci.*, 1989, **132**, 43.

- 9 F. Elias, J. C. Bacri, C. Flament, E. Janiaud, D. Talbot and W. Drenckhan-Andreatta, *et al.*, Magnetic soap films and magnetic soap foams, *Colloids Surf., A*, 2005, **263**, 65.
- 10 W. Drenckhan-Andreatta, F. Elias, S. Hutzler, D. Weaire, E. Janiaud and J. C. Bacri, Bubble size control and measurement in the generation of ferrofluid foams, *J. Appl. Phys.*, 2003, **93**, 10078.
- 11 J. C. Bacri and F. Elias, Ferrofluids: A Model System of Self-Organised Equilibrium, in *Morphogenesis: Origins of Patterns and Shapes*, ed. P. Bourguin, A. Lesne, Springer Berlin Heidelberg, Berlin, Heidelberg, 2011. p. 15.
- 12 M. D. Cowley and R. E. Rosensweig, The interfacial stability of a ferromagnetic fluid, *J. Fluid Mech.*, 1967, **30**, 671.
- 13 H. Knieling, R. Richter, I. Rehberg, G. Matthies and A. Lange, Growth of surface undulations at the Rosensweig instability, *Phys. Rev. E*, 2007, **76**, 066301.
- 14 J. C. Bacri and D. Salin, Instability of ferrofluid magnetic drops under magnetic field, *J. Phys., Lett.*, 1982, **43**, L-649.
- 15 F. Elias, C. Flament, J. C. Bacri and S. Neveu, Macro-Organized Patterns in Ferrofluid Layer: Experimental Studies, *J. Phys. I France*, 1997, **7**, 711.
- 16 J. V. I. Timonen, M. Latikka, L. Leibler, R. H. A. Ras and O. Ikkala, Switchable Static and Dynamic Self-Assembly of Magnetic Droplets on Superhydrophobic Surfaces, *Science*, 2013, **341**, 253.
- 17 C. Rigoni, M. Pierno, G. Mistura, D. Talbot, R. Massart and J. C. Bacri, *et al.*, Static Magnetowetting of Ferrofluid Drops, *Langmuir*, 2016, **32**, 7639.
- 18 C. Rigoni, S. Bertoldo, M. Pierno, D. Talbot, A. Abou-Hassan and G. Mistura, Division of Ferrofluid Drops Induced by a Magnetic Field, *Langmuir*, 2018, **34**, 9762.
- 19 M. Latikka, M. Backholm, A. Baidya, A. Ballesio, A. Serve and G. Beaune, *et al.*, Ferrofluid Microdroplet Splitting for Population-Based Microfluidics and Interfacial Tensiometry, *Adv. Sci.*, 2020, **7**, 2000359.
- 20 S. Shyam, P. K. Mondal and B. Mehta, Field driven evaporation kinetics of a sessile ferrofluid droplet on a soft substrate, *Soft Matter*, 2020, **16**, 6619.
- 21 S. Shyam, P. K. Mondal and B. Mehta, Magnetofluidic mixing of a ferrofluid droplet under the influence of a time-dependent external field, *J. Fluid Mech.*, 2021, **917**, A15.
- 22 L. B. King, E. Meyer, M. A. Hopkins, B. S. Hawkett and N. Jain, Self-Assembling Array of Magneto-electrostatic Jets from the Surface of a Superparamagnetic Ionic Liquid, *Langmuir*, 2014, **30**, 14143.
- 23 C. A. Schneider, W. S. Rasband and K. W. Eliceiri, NIH Image to ImageJ: 25 years of image analysis, *Nat. Chem. Biol.*, 2012, **9**, 671.
- 24 M. Beleggia, D. Vokoun and M. De Graef, Demagnetization factors for cylindrical shells and related shapes, *J. Magn. Magn. Mater.*, 2009, **321**, 1306.
- 25 G. I. Barenblatt, *Scaling, Self-similarity, and Intermediate Asymptotics*, Cambridge University Press, Cambridge, UK, 1996.
- 26 P. G. de Gennes, F. Brochard-Wyart and D. Quéré, *Gouttes, bulles, perles et ondes*, Édition Belin, Paris, France, 2005.